Acta Mechanica Sinica (2012) 28(5):1389–1397
DOI 10.1007/s10409-012-0145-0

RESEARCH PAPER

Numerical analysis of confinement effect on crack propagation mechanism from a flaw in a pre-cracked rock under compression

Amin Manouchehrian · Mohammad Fatehi Marji

Received: 22 February 2012 / Revised: 20 April 2012 / Accepted: 16 May 2012

Abstract In many situations rocks are subjected to biaxial loading and the failure process is controlled by the lateral confinement stresses. The importance of confinement stresses has been recognized in the literature by many researchers, in particular, its influence on strength and on the angle of fracture, but still there is not a clear description for the influence of confining stress on the crack propagation mechanism of rocks. This paper presents a numerical procedure for the analysis of crack propagation in rock-like materials under compressive biaxial loads. Several numerical simulations of biaxial tests on the rock specimen have been carried out by a bonded particle model (BPM) and the influence of confinement on the mechanism of crack propagation from a single flaw in rock specimens is studied. For this purpose, several biaxial compressive tests on rectangular specimens under different confinement stresses were modeled in (2 dimensional particle flow code) PFC^{2D}. The results show that wing cracks initiate perpendicular to the flaw and trend toward the direction of major stress, however, when the lateral stresses increase, this initiation angle gets wider. Also it is concluded that in addition to the material type, the initiation direction of the secondary cracks depends on confinement stresses, too. Besides, it is understood that secondary cracks may be produced from both tensile and shear mechanisms.

Keywords Crack propagation · Confinement · Bonded particle model · Rock · Secondary cracks

1 Introduction

In addition to elasticity and material mechanics theories, over the past century several failure criteria such as Rankin, Griffith, Saint–Venant, Drucker–Prager, Mohr–Coulomb, Hoek–Brown and etc. have been presented to describe fracture phenomena due to stress concentration in materials. Sometimes an engineering structure seems to be stable and safe according to elasticity theory, material mechanics theory and failure criteria, but due to pre-existing cracks or induced cracks during loadings, it yields at lower level of stress in which this sudden failure can lead to heavy losses.

As viewed from structural point, a rock is made up of minerals and cements with numerous microcracks and pores in which various combinations of these elements result in various properties (physical properties, chemical properties, mechanical properties, magnetic properties, etc.) [1–6]. Studies have shown that large-scale behavior of failure process in rocks is strongly affected by behavior of microcracks (initiation, propagation and coalescence) [7–9]. So it is very important to understand the mechanism of microcrack's growth under different loading situations. For example, for rock slope stability it is essential to know if and how the existing fractures connect with each other or coalesce to form a continuous fracture surface. This problem has attracted many researchers to study in the field of rock crack behaviors under different loading situations [10–18].

In recent years, many studies have been done to understand crack propagation mechanism in rocks and rock-like materials under uniaxial load [11–17]. Results have shown different crack patterns, but there is a common characteristic in all of these researches [14]. Cracks propagate in rocks and rock-like materials in two forms: wing cracks and secondary cracks. Wing cracks are tensile cracks that initiate at the tips of pre-existing cracks (flaws) and propagate in a stable manner towards the direction of the maximum compressive stress. Secondary cracks initiate also from the tips of the flaws, propagate in a stable manner, and have been recognized by many researchers as shear cracks. Two initiation directions are possible for secondary cracks: one coplanar or quasi-coplanar to the flaw, and the other one parallel to the wing cracks but in the opposite direction [11–13]. In par-

A. Manouchehrian (✉$_1$)· M. F. Marji (✉$_2$)
Mining and Metallurgical Engineering Department,
Yazd University, Yazd, Iran
e-mail$_1$: amin.manouchehrian@gmail.com
e-mail$_2$: mfatehi@yazduni.ac.ir

ticular, Wong and Einstein considering previous studies presented a systematic evaluation of cracking behavior in specimens containing single flaws which are subjected to uniaxial compression [14].

In many situations rocks are subjected to biaxial loads (for example in the walls of tunnels), so mechanism of failure and crack growth under biaxial loads can be very helpful, but these kinds of studies have been done by few researchers especially in the area of rock mechanics [19–24]. Experimental studies by Kupfer et al. [19] on concrete samples under both uniaxial and biaxial compression using different stress ratios showed generation of numerous microcracks parallel to the applied load. The results showed that the complete collapse of specimen was associated with the formation of several shear fractures induced at angles between 18° and 30° from the loading plate [19]. Tayler et al. [20] performed a series of biaxial compressive tests on cubic samples of all-lightweight aggregate concrete. They reported splitting of specimens into thin slabs parallel to unstressed direction without formation of shear fractures. Similar observations were reported by Brown [21] who performed biaxial tests on marble samples. Papamichis et al. [22] tested rock samples, rigidly confined laterally in one plane. The results showed that the failure mode depends on the type of rock; Berea sandstone samples failed by splitting parallel to the unconfined surfaces and Indiana limestone failed by shearing. Fracture surfaces parallel to intermediate principal stress direction were observed by Mogi [23] who tested prismatic rock samples using tapered greased epoxy cement inserts. Sahouryeh et al. [24] presented an experimental and analytical investigation into three-dimensional crack growth under biaxial compression and reported that all samples failed by splitting parallel to the free surface.

There are various numerical methods for analyzing crack initiation and propagation such as finite element method (FEM), boundary element method (BEM), displacement discontinuity method (DDM) and discrete element method (DEM) [25–28]. Recently, a numerical simulation code, 2 dimensional rock failure process analysis ($RFPA^{2D}$), has been released for the analysis of crack propagation in rock which is capable of modeling both global failure of rock and local cracking at flaw tips [29]. Also failure process and cracking in rock and rock-like materials have been modeled by many researchers by bonded particle model (BPM) using particle flow code (PFC) [30–35]. In this code cracks generate simply by breakage of bonds between circular particles instead of solving complex mathematical equations related to fracture mechanics.

In this paper confining stress influence on crack growth from a flaw in rocks as a brittle material is numerically studied. The numerical results can be very useful for recognition of mechanism of growth and coalescence of cracks in the rock mass. In rock engineering projects where pre-existing cracks (finite cracks) play a dominant role in stability of rock structure, such results can improve stability analyses and make the structure safer.

2 Theory

Pre-existed cracks in rocks and rock-like materials under compressive loads grow and coalesce to form fracture planes. Many researchers have studied on the analytical problem of crack initiation and propagation from pre-existing cracks under compressive loads [36, 37].

Fracture mechanics-based analysis of crack in two-dimensions is very common in literatures. Fracture mechanics can be divided into linear elastic fracture mechanics (LEFM) and elasto-plastic fracture mechanics (EPFM). LEFM gives very good results for brittle elastic materials and is a primary requirement for brittle rock material analysis. For a given defect, crack propagation may be accomplished in opening mode (Mode-I), shearing mode (Mode-II), and tearing mode (Mode-III) (Fig. 1).

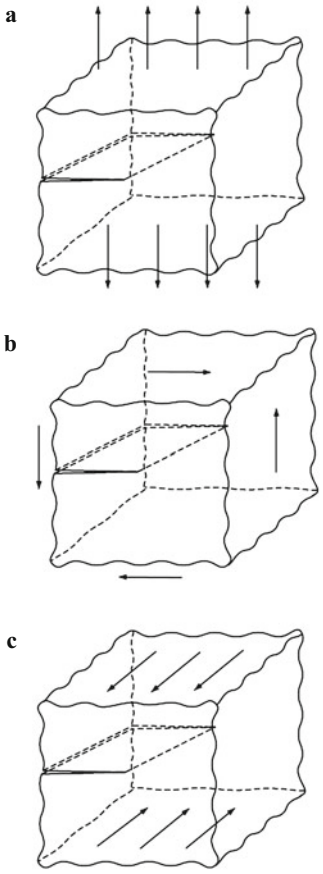

Fig. 1 Basics modes of crack extension: **a** Opening mode (Mode-I); **b** Shearing mode (Mode-II); **c** Tearing mode (Mode-III)

Practical engineering cracked structures are usually subjected to mixed mode loading and in general the stress intensity factors in Mode-I and Mode-II are both nonzero. Using Irwin's concept of the stress intensity factors, which characterize the strength of the singularity at a crack tip of length l (Fig. 2), the near crack tip ($r \ll l$) stresses (Eqs. (1)–(3)) and

displacements (Eqs. (4) and (5)) in the mixed mode conditions are always expressed as [38]

$$\sigma_{xx} = \frac{K_{\mathrm{I}}}{\sqrt{2\pi r}}\cos\frac{\theta}{2}\left(1-\sin\frac{\theta}{2}\sin\frac{3\theta}{2}\right) - \frac{K_{\mathrm{II}}}{\sqrt{2\pi r}}\sin\frac{\theta}{2}\left(2+\cos\frac{\theta}{2}\cos\frac{3\theta}{2}\right), \quad (1)$$

$$\sigma_{yy} = \frac{K_{\mathrm{I}}}{\sqrt{2\pi r}}\cos\frac{\theta}{2}\left(1+\sin\frac{\theta}{2}\sin\frac{3\theta}{2}\right) + \frac{K_{\mathrm{II}}}{\sqrt{2\pi r}}\sin\frac{\theta}{2}\cos\frac{\theta}{2}\cos\frac{3\theta}{2}, \quad (2)$$

$$\tau_{xy} = \frac{K_{\mathrm{I}}}{\sqrt{2\pi r}}\sin\frac{\theta}{2}\cos\frac{\theta}{2}\cos\frac{3\theta}{2} + \frac{K_{\mathrm{II}}}{\sqrt{2\pi r}}\cos\frac{\theta}{2}\left(1-\sin\frac{\theta}{2}\sin\frac{3\theta}{2}\right), \quad (3)$$

$$\mu_x = \frac{K_{\mathrm{I}}}{2\mu}\sqrt{\frac{r}{2\pi}}\cos\frac{\theta}{2}\left(K-1+2\sin^2\frac{\theta}{2}\right) + \frac{K_{\mathrm{II}}}{2u}\sqrt{\frac{r}{2\pi}}\sin\frac{\theta}{2}\left(K+1+2\cos^2\frac{\theta}{2}\right), \quad (4)$$

$$\mu_y = \frac{K_{\mathrm{I}}}{2\mu}\sqrt{\frac{r}{2\pi}}\sin\frac{\theta}{2}\left(K+1-2\cos^2\frac{\theta}{2}\right) - \frac{K_{\mathrm{II}}}{2u}\sqrt{\frac{r}{2\pi}}\cos\frac{\theta}{2}\left(K-1-2\sin^2\frac{\theta}{2}\right), \quad (5)$$

where $K = 3-4v$ denotes plane strain and $K = (3-v)/(1+v)$ plane stress and μ is the shear modulus (often referred to as strain energy release rate (G)).

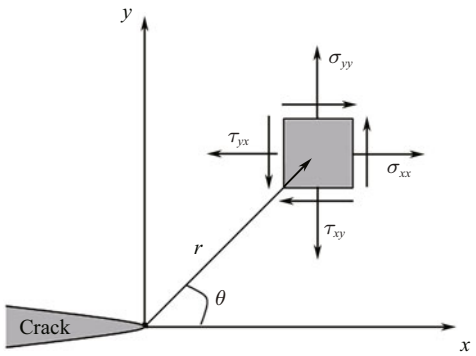

Fig. 2 Definition of the coordinate axis ahead of a crack tip used for a two dimensional deformation field

In reality, cracks in brittle materials under compression grow and coalesce with adjacent cracks, but due to some factors, these analytic models are not able to precisely model crack propagation mechanism. In order to make further progress in developing analytical and computational models for failure of brittle solids under compression, experimental and appropriate numerical (e.g., RFPA^{2D} and PFC) studies can be helpful to understand the stress state faces and can also present a powerful criterion for the initiation and propagation of cracks.

3 Numerical simulation

3.1 Model generation

In the numerical simulation by PFC^{2D}, rock material is represented by an assembly of rigid circular disks bonded together at their contact points. PFC contains two bonding models: a contact-bond model and a parallel-bond model. The parallel-bond has a finite size that acts over either circular or rectangular cross section between the particles, whereas the contact-bond acts only at the contact point due to its vanishingly small size, which can be embodied with the parallel-bond of radius zero. Therefore, the contact-bond can only resist the force acting at the contact, while the parallel-bond can resist both the force and moment. The parallel-bonds are activated with five parameters, such as normal and shear bond strength, normal and shear bond stiffness, and the bond radius, among which the bond stiffness and bond radius are not signed as in the contact-bond model. The contact/parallel-bonds are broken if the applied stresses are larger than the bond strengths [39, 40]. In the contact-bond model, bond breakage may not affect the macro stiffness significantly provided the particles remain in contact. However, in the parallel-bond model, bond breakage induces an immediate decrease in macro stiffness because the stiffness is contributed by both contact stiffness and bond stiffness. Therefore, the parallel-bond model can be more realistic for rock-like material modeling in which the bonds may break in either tension or shearing with an associated reduction in stiffness [41]. So, the parallel-bond model is chosen for rock simulation in this investigation. A parallel-bond model is defined by five micro parameters consisting of: normal and shear stiffness (k_{n}) and (k_{s}) (stress/displacement); normal and shear strength (σ_c) and (τ_c) (stress); and bond radius (R). These micro parameters should be adjusted to reproduce the macro properties of the real specimen under uniaxial compression such as Young's modulus, UCS, and Poisson's ratio and this adjustment is done by a calibration process. The calibration is a "trial and error" process in which by changing micro parameters in simulated biaxial or Brazilian tests, the laboratory values of macro parameters (Young's modulus, UCS, and Poisson's ratio) will be reproduced. When simulated results and laboratory results are the same, the applied micro parameters will be set as input for numerical simulation. Also there are some quantitative techniques for the selection of micro parameters [42]. In this study, calibration process is done by simulating a biaxial test.

3.2 Simulation of compressive loading

The biaxial compressive test, shown in Fig. 3 is to be simulated to analyze confining stress effect on mechanism of crack propagation from a single flaw in rock. Physical and mechanical properties of the simulated rock specimen

are summarized in Table 1. Also Table 2 presents the selected microparameters for numerical simulation by PFC^{2D}. The specimen has the height of $H = 12$ cm and width of $W = 6$ cm. The PFC^{2D} model of the biaxial test is given in Fig. 4. After reproduction of specimen, the flaw is generated by deleting the particles in an appropriate region. Another method to generate the flaw is to set the strength of the particles between adjacent particles in the flaw surface to zero. Nohut modeled the notch in the single-edge-notched beam (SENB) test with both methods and observed the same results [32]. It is reasonable because the radius of the notch tip is not determined by the radius of the particle which is deleted or whose bond strength is assigned to zero but it is determined by the radius, the location and the arrangement of the particle pair which stay just above the notch. Therefore it does not have any effect on the crack sharpness. The flaw has a length of 3.0 cm ($w/a = 4$) which locates with an angle of 45° in the center of the specimens and the opening of the flaw is 1.5 mm. Four walls of the model plays role of platens and confinement pressure. Specifically, the lower wall is fixed and the upper wall moves down with a velocity of V_p to simulate loading platen and the lateral stresses are imposed by the right and left walls. And then, several simulations of biaxial test with different confining stresses (0, 5, 10, 30 and 50 MPa) are performed.

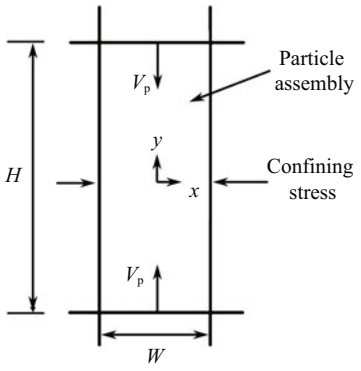

Fig. 3 Schematic representation of biaxial compressive test

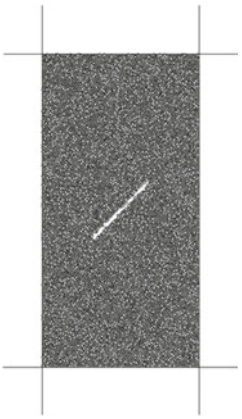

Fig. 4 PFC^{2D} model of a rock specimen with a single flaw in compressive test

Table 1 Physical and mechanical properties of simulated rock

Properties	Value
Density/(kg · m^{-3})	2 700
Young's modulus/GPa	55.5
Uniaxial compressive strength/MPa	145
Tensile strength/MPa	47.60
Poisson's ratio	0.27

Table 2 Microparameters used for the PFC^{2D} model

Microparameters	Value
Particle mean radius/mm	0.4
Particle radius ratio, R_{max}/R_{min}	1.66
Particle density/(kg · m^{-3})	2 700
Particle contact modulus, E_c/GPa	44.5
Particle stiffness ratio, k_n/k_s	1.0
Parallel-bond radius multiplier	1.0
Parallel-bond modulus, E_c/GPa	44.5
Parallel-bond stiffness ratio, k_n/k_s	1.0
Particle friction coefficient	0.50
Parallel-bond normal strength, mean/MPa	177.8
Parallel-bond normal strength, std. dev./MPa	45
Parallel-bond shear strength, mean/MPa	177.8
Parallel-bond shear strength, std. dev./MPa	45

3.3 Results

To study confinement effect on crack propagation mechanism from a single flaw, several numerical simulations are carried out for the specimens. The specimens are subjected to different confining stresses: 0, 5, 10, 30 and 50 MPa. Table 3 shows the values of axial and confinement stresses at different stages of simulation (75% peak stress, 90% peak stress, peak stress, 90% post-peak stress and 80% post-peak stress).

The failure developments for specimens under compressive loads are illustrated in Figs. 5–9. The light and dark lines denote the tensile and shear microcracks in the PFC^{2D} model, respectively.

Under unconfined situation, first noticeable fractures appear as wing cracks. At about 75% of peak-stress wing cracks initiate perpendicularly to the flaw surface from both tips and turn toward loading direction as the stresses increase. Secondary cracks propagate from the flaw tips quasi-coplanar to it. Failure of specimen is caused by the growth of secondary cracks in the post peak-stress stage.

Table 3 Values of axial and confinement stresses at different stages of simulation

Confinement stress/MPa	Axial stress/MPa				
	75% peak	90% peak	Peak	90% post-peak	80% post-peak
0	109.3	131.1	145.7	131.1	116.5
5	127.5	153.0	170.0	153.0	136.0
10	131.6	158.0	175.5	158.0	140.4
30	145.0	174.0	193.3	174.0	154.6
50	166.0	199.3	221.4	199.3	177.2

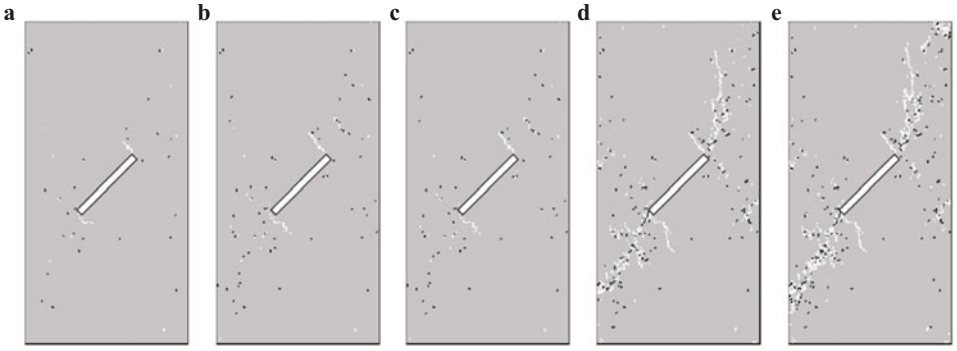

Fig. 5 Crack propagation from a single flaw at confinement of 0 MPa. **a** 75% peak; **b** 90% peak; **c** peak; **d** 90% post-peak; **e** 80% post-peak

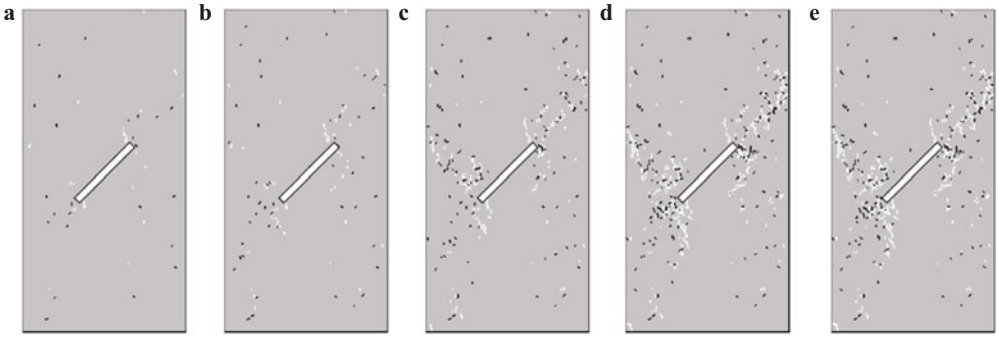

Fig. 6 Crack propagation from a single flaw at confinement of 5 MPa. **a** 75% peak; **b** 90% peak; **c** peak; **d** 90% post-peak; **e** 80% post-peak

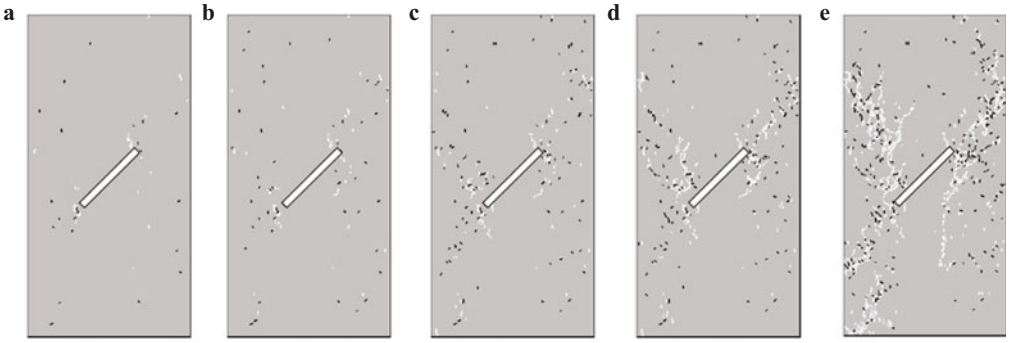

Fig. 7 Crack propagation from a single flaw at confinement of 10 MPa. **a** 75% peak; **b** 90% peak; **c** peak; **d** 90% post-peak; **e** 80% post-peak

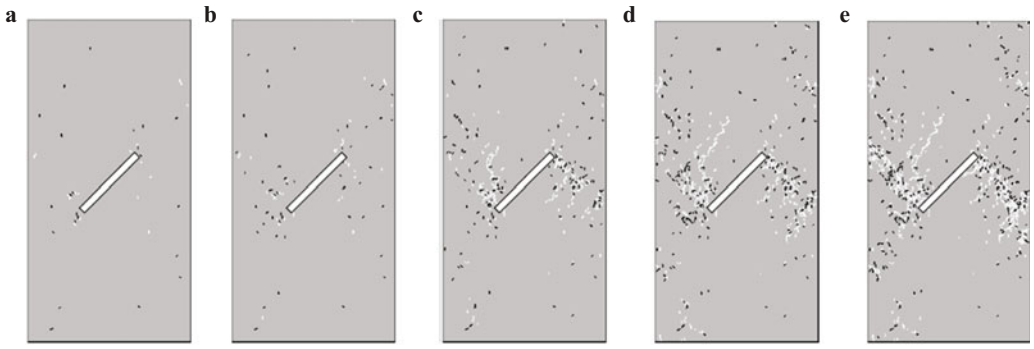

Fig. 8 Crack propagation from a single flaw at confinement of 30 MPa. **a** 75% peak; **b** 90% peak; **c** peak; **d** 90% post-peak; **e** 80% post-peak

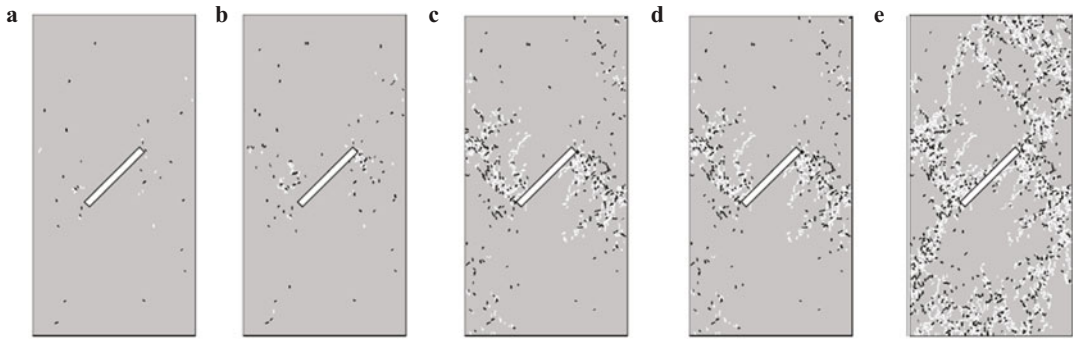

Fig. 9 Crack propagation from a single flaw at confinement of 50 MPa. **a** 75% peak; **b** 90% peak; **c** peak; **d** 90% post-peak; **e** 80% post-peak

Similarly, wing cracks begin to form at near peak-stress under confinement of 5 MPa. In this condition, initiation angles of wing cracks are not perpendicular to the flaw surface. In fact, the angle between the maximum load direction and the initial direction of wing crack become sharper. Due to confining stresses, wing cracks detain and can not propagate as far as in the case where there is no confinement, so wing cracks are shorter than those in unconfined condition. Both the cracks coplanar with the flaw and the ones parallel with the flaw but in opposite direction of wing cracks are seen as secondary cracks. In addition to these, branching of secondary cracks is obvious in the case of 10 MPa lateral stresses.

For the confinement of 30 MPa, wing cracks are very short and stop at very early stage after initiation. Wider secondary cracks parallel with wing cracks but in opposite direction are conspicuous. Besides, fractures appear at top and bottom of the specimen for the confinement of 50 MPa case.

4 Discussion

The experimental and numerical studies in rocks and rock-like materials show two types of cracks: wing cracks and secondary cracks. Both types of cracks may initiate at the tips of the flaws and propagate in a stable manner and the secondary cracks may also initiate at the kinked part of the propagated original crack or previously existent secondary cracks. Wing cracks initiate at an angle with the flaw and tend to propagate towards the direction of the maximum compressive stress. Secondary cracks, however, have been observed to initiate in a direction coplanar or quasi-coplanar to the flaw and also parallel to the wing cracks but in the opposite direction. The quasi-coplanar direction has been systematically observed in a large number of tests, while the second direction has been observed only in few tests. It is concluded by many researchers that the initiation direction of the secondary cracks may depends on the material type [11–13]. According to Figs. 5–9, the current numerical results show that the secondary cracks may form in both directions in the same material. In fact, the confining stresses may have great influence on the initiation direction of the secondary cracks. So according to the present work, in addition to material type the initiation direction of secondary cracks can be depended on the confinement stresses, too.

In most fracture mechanics literatures, the secondary cracks are described as shear cracks or shear zones [11–13], but some experimental and numerical works show that the secondary cracks can be produced from both shear and tensile stresses [17, 37]. The particles displacement vectors are shown in Fig. 10, demonstrating the direction of the particles displacement and crack opening or sliding under uniaxial loading. As is illustrated, wing cracks start when bonds

between particles (at the tips of the flaw) break and these zones start to split in opening mode (Fig. 10a). Actually, induced tensile stresses lead to initiation of wing cracks but increase of confining stresses weaken this induction. So, no more wing cracks initiate when the confining stresses are high enough to completely offset this effect. Increase of the major stress closes the wing cracks, but new cracks (secondary cracks) initiate due to breakage of the bonds between particles by induced tensile stresses (Fig. 10b). These cracks can propagate from the tips of the flaw in different directions (Figs. 10b and 11). Also, the particle displacement vectors illustrate secondary cracks initiation at the confinement of 50 MPa (Fig. 11). This shows that secondary cracks initiate under tensile stresses (Fig. 11a) but they will be subjected to shear forces (Fig. 11b) later. These shear forces may cause roughness and uncleanness of the crack surface. It is said while wing cracks show a clean and smooth surface, the surface of shear cracks appears rough and covered with powder, which is an indication of slip between the faces of the crack [11]. These reasons which are derived from experimental works have ever served as the main reasons for recognizing the secondary cracks as shear cracks, but the present numerical work shows that this conclusion may be not correct.

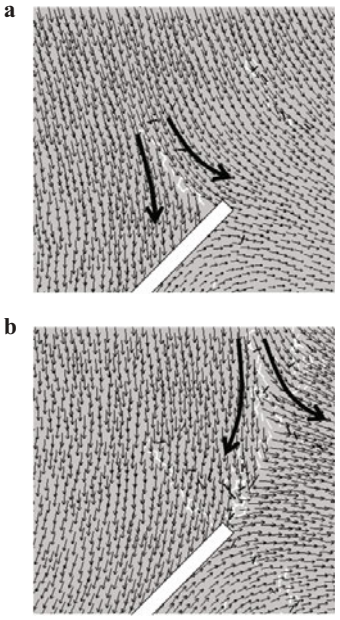

Fig. 10 The particle displacement vectors showing initiation of **a** wing cracks (at 90% peak stress) and **b** secondary cracks (at peak stress) under uniaxial compressive loading

Therefore, crack propagation from a single flaw in rocks and rock-like materials can be explained as follows:

Wing cracks start from tips of the flaw in opening mode due to the induced tensile stresses and continue up to the zones where the induced tensile stresses are not high enough to break bonds between the particles. At this situation, secondary cracks start under similar mechanism (in opening mode) but they may be subjected to shear forces later. Also, crack branching may occur. It means that new branches of crack initiate to reduce strain energy inside the specimen when induced tensile stresses or shear stresses are not high enough for the propagation of the currently growing crack.

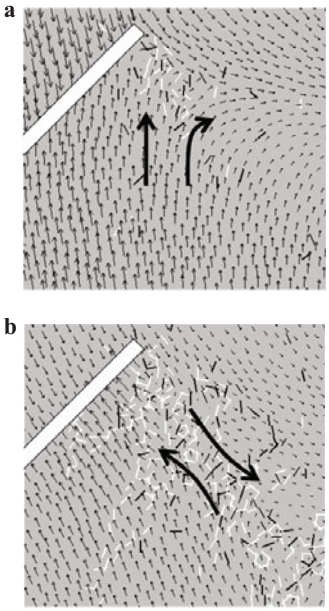

Fig. 11 The particle displacement vectors showing secondary cracks initiation at **a** 90% peak stress and **b** peak stress in the confinement of 50 MPa

5 Conclusions

In this paper, the effect of confinement on crack propagation from a single flaw in rock was numerically investigated. For this purpose several simulations have been performed to study failure process under lateral stresses of 0, 5, 10, 30 and 50 MPa. The following results and conclusions can be drawn from the present study.

Some common characteristics of failure development resulting from numerical simulations are quite similar to laboratory observations. These characteristics can be described as:

(a) Initial micro cracks form in the pre-failure stage due to the existence of flaw, and their development are highly affected by stress concentration around the flaw;

(b) Fractures take place near peak stresses;

(c) Fracture planes or faults appear in the post-failure stage and cause the specimen to fail.

The numerical simulation results show that the initiation of wing and secondary cracks and the failure process are strongly affected by the confining stresses. In the absence of confining stresses, wing cracks form perpendicular to flaw and tend toward loading direction. As the confinement stresses increase, wing cracks initiate in a wider

angle with respect to the original flaw. Increase of confining stresses leads to shortening of wing cracks and when these stresses are sufficiently high, wing cracks become completely negligible.

The numerical results also show that from tips of the flaw, secondary cracks propagate in two directions; one coplanar or quasi-coplanar to the flaw, and the other one parallel to the wing cracks but in the opposite direction. Secondary cracks propagate only quasi-coplanar to the flaw in unconfined situation but the second direction of propagation appears when the confinement stress increases. It is understood that in addition to the type of material, the magnitude of confinement can also affect the direction of secondary cracks propagation. Due to increase of confining stresses, the axial fractures detain and more shear fractures develop and coalesce to form shear faults. Furthermore, higher applied confinement will cause wider shear fault plane.

In many literatures, the secondary cracks are described as shear cracks but the current numerical work has shown that these kinds of cracks can be produced by tensile mechanism, too. In fact, from this work it can be concluded that secondary cracks are produced under tensile forces but these cracks may be subjected to shear forces which can make the crack surface rough and unclean. So, under compressive loading conditions, the initiation of secondary cracks may be attributed to both shear and tensile mechanisms.

References

1 Brace, W. F.: Dependence of fracture strength of rocks on grain size. Bulletin of Mineral Industries Experiment Station. Mining Engineering Series. Rock Mech. **76**, 99–103 (1961)

2 Fahy, M. P., Guccione, M. J.: Estimating strength of sandstone using petrographic thin-section data. Bull. Assoc. Eng. Geol. **16**, 467–485 (1979)

3 Shakoor, A., Bonelli, R.E.: Relationship between petrographic characteristics, engineering index properties and mechanical properties of selected sandstones. Bull. Assoc. Eng. Geol. **28**, 55–71 (1991)

4 Edet, A.: Physical properties and indirect estimation of microfractures using Nigerian carbonate rocks as examples. Eng. Geol. **33**, 71–80 (1992)

5 Howarth, D. F., Rowlands, J. C.: Quantitative assessment of rock texture and correlation with drillability and strength properties. Rock Mech. Rock Eng. **20**, 57–85 (1987)

6 Manouchehrian, A., Sharifzadeh, M., Hamidzadeh, R.: Application of artificial neural networks and multivariate statistics to estimate UCS using textural characteristics. Int. J. Min. Sci. Technol. **22**, 229–236 (2012)

7 Besuelle, P., Desrues, J., Raynaud, S.: Experimental characterisation of the localisation phenomenon inside a Vosges sandstone in a triaxial cell. Int. J. Rock Mech. Min. Sci. **37**, 1223–1237 (2000)

8 El Bied A., Sulem, J., Martineau, F.: Microstructure of shear zones in Fontaine bleau sandstone. Int. J. Rock Mech. Min. Sci. **39**, 917–932 (2002)

9 Labuz, J. F., Biolzi, L.: Experiments with rock: remarks on strength and stability issues. Int. J. Rock Mech. Min. Sci. **44**, 525–537 (2007)

10 Vallejo, L. E.: The influence of fissures in a stiff clay subjected to direct shear. Geotechnique **37**, 69–82 (1987)

11 Park, C. H., Bobet, A.: Crack initiation, propagation and coalescence from frictional flaws in uniaxial compression. Engineering Fracture Mechanics **77**, 2727–2748 (2010)

12 Bobet, A., Einstein, H. H.: Fracture coalescence in rock-type materials under uniaxial and biaxial compression. Int. J. Rock Mech. Min. Sci. **35**, 863–888 (1998)

13 Bobet, A., Einstein, H. H.: Numerical modeling of fracture coalescence in a model rock material. Int. J. Fracture **92**, 221–252 (1998)

14 Wong, L. N. Y., Einstein, H. H.: Systematic evaluation of cracking behavior in specimens containing single flaws under uniaxial compression. Int. J. Rock Mech. Min. Sci. **46**, 239–249 (2009)

15 Wong, R. H. C., Chau, K. T.: Crack coalescence in a rock-like material containing two cracks. Int. J. Rock Mech. Min. Sci. **35**, 147–164 (1998)

16 Mughieda, O., Alzo'ubi, A. K.: Fracture mechanisms of offset rock joints – A laboratory investigation. Geooth. Geol. Eng. J. **22**, 545–562 (2004)

17 Fatehi Marji, M., Gholamnejad, J., Eghbal, M.: On the crack propagation mechanism of brittle rocks under various loading conditions. In: Proceedings of International Multidisciplinary Scientific GeoConference, Bulgaria, 561–568 (2011)

18 Vallejo, L.E.: The brittle and ductile behavior of clay samples containing a crack under mixed mode loading. Theor. Appl. Fract. Mech. **10**, 73–78 (1988)

19 Kupfer, H., Hilsdorf, H. K., Rusch, H.: Behaviour of concrete under biaxial stresses. ACI J. **66**, 656–66 (1969)

20 Tayler, M. A., Jain, A. K., Ramey, M. R.: Path dependent biaxial compressive testing of an all-lightweight aggregate concrete. J. Am. Concr. Inst. **69**, 758–64 (1972)

21 Brown, E. T.: Fracture of rock under biaxial compression. In: Proceedings of the 3rd Congress of the International Society of Rock Mechanics, Advances in Rock Mechanics, Denver, Washington (DC), 111–117 (1974)

22 Papamichos, E., Labuz, J. F., Vardoulakis, I.: A surface instability detection apparatus. Rock Mech. Rock Eng. **27**, 37–56 (1994)

23 Mogi, K.: Effects of intermediate principal stress on rock failure. J. Geophys. Res. **72**, 5117–5131 (1967)

24 Sahouryeh, E., Dyskin, A. V.: Crack growth under biaxial compression. Engineering Fracture Mechanics **69**, 2187–2198 (2002)

25 Ingraffea, A. R., Heuze, F. E.: Finite element models for rock fracture mechanics. Int. J. Numer. Anal. Meth. Geomech. **4**, 25–43 (1980)

26 Fatehi Marji, M., Dehghani, I.: Kinked crack analysis by a hybridized boundary element/boundary collocation method. Int. J. Solids and Structures **47**, 922–933 (2010)

27 Fatehi Marji, M., Hosseini-nasab, H., Kohsary, A. H.: A new cubic element formulation of the displacement discontinuity method using three special crack tip elements for crack analysis. JP J. Solids and Structures **43**, 61–91 (2007)

28 Tang, C. A., Lin, P., Wong, R. H. C., et al.: Analysis of crack coalescence in rock-like materials containing three flaws – Part II: Numerical approach. Int. J. Rock Mech. Min. Sci. **38**, 925–939 (2001)

29 Li, Y. P., Chen, L. Z., Wang, Y. H.: Experimental research on pre-cracked marble under compression. Int. J. Solids and Structures **42**, 2505–2516 (2005)
30 Lee, H., Jeon, S.: An experimental and numerical study of fracture coalescence in pre-cracked specimens under uniaxial compression. Int. J. Solids and Structures **48**, 979–999 (2011)
31 Ma, W., Wang, X.J., Ren, F.: Numerical simulation of compressive failure of heterogeneous rock-like materials using SPH method. Int. J. Rock Mech. and Min. Sci. **48**, 353–363 (2011)
32 Nohut, S.: Prediction of crack-tip toughness of alumina for given residual stresses with parallel-bonded-particle model. Computational Materials Science **50**, 1509–1519 (2011)
33 Yoonetal, J. S.: Simulating fracture and friction of Aue granite under confined asymmetric compressive test using clumped particle model. Int. J. Rock Mech. Min. Sci. **49**, 68–83 (2012)
34 Zhang, X. P., Wong, L. N. Y.: Cracking processes in rock-like material containing a single flaw under uniaxial compression: A numerical study based on parallel bonded-particle model approach. Rock Mech. and Rock Eng. **45**, 711–737 (2011)
35 Asadi, M. S., Rasouli, V., Barla, G.: A bonded particle model simulation of shear strength and asperity degradation for rough rock fractures. Rock Mech. Rock Eng. **45**, 649–675 (2012)
36 McClintock, F. A., Walsh, J. B.: Friction on Griffith crack under pressure. In: Proceedings of the Fourth US National Congress on Applied Mechanics, New York, 1015–1021 (1962)
37 Horii, H., Nemat-Nasser, S.: Brittle failure in compression: splitting, faulting and ductile–brittle transition. Philos. Trans. R. Soc. Lond. A **319**, 337–374 (1986)
38 Ashby, M. F., Sammis, C. G.: The damage mechanics of brittle solids in compression. Pure Appl. Geophys. **133**, 489–521 (1990)
39 Itasca, C. G.: Users' Manual for Particle Flow Code in 2 Dimensions (PFC^{2D}), Version 3.1. Minneapolis Minnesota (2002)
40 Potyondy, D. O., Cundall, P. A.: A bonded-particle model for rock. Int. J. Rock Mech. Min. Sci. **41**, 1329–1364 (2004)
41 Cho, N., Martin, C. D., Sego, D. C.: A clumped particle model for rock. Int. J. Rock Mech. Min. Sci. **44**, 997–1010 (2007)
42 Yoon, J.: Application of experimental design and optimization to PFC model calibration in uniaxial compression simulation. Int. J. Rock Mech. Min. Sci. **44**, 871–889 (2007)